Journal of Sound and Vibration (1988) **124**(1), 55–78

PERIODIC MOTIONS AND BIFURCATIONS IN DYNAMICS OF AN INCLINED IMPACT PAIR

M. S. HEIMAN

Hughes Aircraft Company, Tucson, Arizona 85704, *U.S.A.*

A. K. BAJAJ AND P. J. SHERMAN

School of Mechanical Engineering, Purdue University, West Lafayette, Indiana 47907, *U.S.A.*

(*Received* 13 *May* 1987, *and in revised form* 6 *October* 1987)

The dynamics of an inclined impact pair, consisting of a harmonically moved primary mass and a secondary mass moving in an inclined slot within the primary mass is investigated in considerable detail. The dynamics of the secondary mass for K impacts in L cycles of the base motion is formulated in terms of a return map. Steady state $K : L$ motions, their stability, and subsequent bifurcations are studied via this map. It is shown that harmonic, subharmonic, and chaotic motions can exist for various values of parameters. Results are presented in the form of stability charts in parameter planes. For a given system parameters set, different types of stable $K : L$ motions as well as chaotic motions can co-exist. Some of the steady state solutions of the return map may be non-viable and may penetrate the wall of the slot. An algorithm is developed to predict the viability boundaries in the parameter plane.

1. INTRODUCTION

Clearances in mechanical systems often occur at joints, linkages, and gear trains, and may be the result of wear, backlash, or manufacturing tolerances. In such situations, impacts may occur when the system is subjected to harmonic inputs, leading to excessive wear, scoring, and high noise levels. In order to properly characterize these adverse effects, it is first necessary to investigate the dynamics associated with basic models for impacting systems. Three such models have received the most attention. The impact damper has been studied by Grubin [1], Masri and Caughey [2], Bapat and Sankar [3], Sadek *et al.* [4, 5], and others. The impact oscillator has been investigated by Senator [6], Shaw and Holmes [7], and Shaw [8]. The third model, which is the most basic and is the subject of the present investigation, is the impact pair.

The impact pair consists of a base mass having a prescribed motion, and a secondary mass, whose motion is a result of impacts with the base mass. An example of an impact pair is that of a ball bouncing on a vibrating table. This problem has been studied extensively by Holmes [9] and by Everson [10]. Their analyses rely heavily on the modern theory of dynamical systems, including ideas from the bifurcation theory of maps, which are used to predict the existence of various periodic motions as well as chaotic motions for the bouncing ball.

0022-460X/88/130055+24 $03.00/0 © 1988 Academic Press Limited

Bapat *et al.* [11] and Veluswami *et al.* [12, 13] investigated the horizontal impact pair, in which the base mass undergoes harmonic motion in the horizontal direction and the secondary mass is constrained to move horizontally in a slot within the base mass. The secondary mass impacts with the ends of the slot. For such a system, Bapat *et al.* [11] obtained closed form solutions for steady state motions of the secondary mass with two alternating impacts per cycle of the base motion (2:1 motion). They also formulated the appropriate constraint equations for more complex $K:L$ alternating impact steady state motions and investigated their stability. Pippard [14] has recently given a very nice introduction to the Poincaré mapping approach in studying dynamics via the example of the horizontal impact pair, and has shown the existence of chaotic motions.

The dynamics of an inclined impact pair was studied by Heiman *et al.* [15]. The secondary mass was assumed to move in a slot which is inclined at an angle θ with the horizontal. Their investigation was limited to 2:1 alternating impact motion, and those bifurcating from it.

The present work considers the dynamics of the inclined impact pair in much more generality than in reference [15]. The approach is the same as in reference [15], and is based on the concept of the Poincaré map or a return map [14, 16]. Fixed points of this map correspond to periodic motions of the impact pair. The equations governing both the existence and the stability of any general K impact per L cycle ($K:L$) periodic motion are developed. Center manifold theory [17] forms the basis for the analysis of subsequent bifurcating motions when a $K:L$ motion loses its stability due to changes in the values of system parameters.

Specific examples of 1:1, 2:1 and 3:1 steady state motions are investigated in detail. The simple nature of the governing equations for 1:1 motion allows the dependence of both the existence and stability of solutions on system parameters to be readily observed. More generally, however, this dependence is shown in the form of stability plots for a variety of system parameter combinations. Analysis of the various return maps in conjunction with computer simulation of the system dynamics shows that different types of $K:L$ steady state motions as well as chaotic motions can co-exist for a given set of parameters.

It is well known [4–8] that some of the solutions obtained as fixed points of the return maps or the constraint equations are not physically viable (penetrating orbits [8]). These solutions usually have been eliminated by simulating the system dynamics corresponding to a fixed point, and then checking the motion. This approach is not very elegant. Based on some observations from the simulation results, a new technique is developed here which determines the viability limits in the parameter plane.

2. PHYSICAL SYSTEM

The impact pair to be studied is shown in Figure 1. The primary mass, M, is constrained to have horizontal displacement given by

$$x(t) = A \sin(\omega t + \tau) \tag{1}$$

where the initial phase τ at time $t = 0$ corresponds to an impact at the lower (left) end of the slot. Let $z(t)$ denote the absolute displacement of the secondary mass, m. Its displacement relative to M is then given by

$$y(t) = z(t) - x(t)\cos(\theta); \qquad -d/2 \leqslant y(t) \leqslant d/2, \tag{2}$$

with an impact occuring whenever $|y(t)| = d/2$, where d is the slot length. Energy loss resulting from any impact is modeled by the coefficient of restitution, e, so that relative

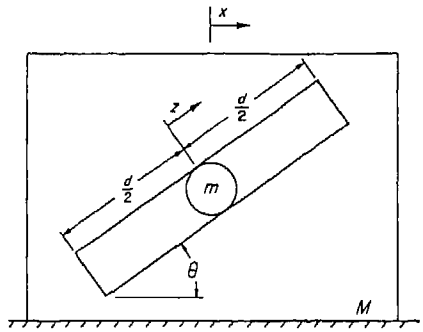

Figure 1. The physical system.

velocities before and after impact are related by

$$\dot{y}_a = -e\dot{y}_b. \tag{3}$$

Finally, between impacts the absolute motion of m is governed by

$$\ddot{z}(t) = -g \sin(\theta). \tag{4}$$

3. METHOD OF ANALYSIS

In order to characterize the evolution of the motion of m it is sufficient to observe the progression of its states when it returns to the lower left end of the slot. This characterization will therefore proceed by using the concept of a first return, or Poincaré map [7, 15]. Let $T_n = \omega t_n$ denote the normalized time instant just prior to a given impact at the left end of the slot, and $\dot{Z}_n$ be the corresponding velocity of m. Then the state of m just prior to impact at the left end of the slot is completely specified by $[T_n, \dot{Z}_n]$. Let $[T_{n+1}, \dot{Z}_{n+1}]$ be the state at the next return of m after having undergone K impacts in exactly L cycles of motion of M. Each of the K impacts between T_n and T_{n+1} will generate two describing equations: one of the motion between consecutive impacts, and the other to account for the impact. Let $\alpha_{n,i} = \omega t_{n,i}$ denote the normalized time instant just prior to an impact for i even, and just after such an impact for i odd. Furthermore, for any variable $f(t)$ denote $f_i = f(\alpha_{n,i})$. Then

$$T_{n+1} = \alpha_{n,2K}, \qquad Z_{n+1} = F[(z_i, \alpha_{n,i}), \quad i = 0, \ldots, 2K], \tag{5a, b}$$

where the functional relation $F[\cdot]$ will presently be developed. In these equations $\alpha_{n,0} = T_n$ and $z_0 = Z_n$. Equations (5) define the mapping

$$[T_{n+1}, \dot{Z}_{n+1}] =: P[T_n, \dot{Z}_n], \tag{6}$$

where P is a two-dimensional return map which completely characterizes the evolution of motion of the secondary mass, within the assumptions made. In particular, P not only depends on the prescribed values of K and L, but also on the type of impact sequence assumed. For example, a 3:1 motion may be either a sequence consisting of two left end impacts followed by a right end impact, one left end impact followed by two right end impacts, or three left end impacts.

The return map P, which we now proceed to characterize, will be used to study both transient and steady state motions of m. Steady state periodic K impact per L cycle motions will be denoted $K:L$ motions. Such motions correspond to fixed points of P, where the range of P is understood to be modulo-$2\pi L$. Note that subharmonic motions

of the type $nK:nL$ correspond to fixed points of the nth iterate of P, namely P^n. The local stability of a $K:L$ motion may be determined by studying the evolution of the transient associated with a perturbation of the corresponding fixed point of P. This information, which is often contained in the Jacobian of P, is developed in the next section.

For notational convenience henceforth $\alpha_{n,i}$ is denoted by simply α_i. During an impact equations (2) and (3), along with the instantaneous impact assumption, imply

$$\alpha_{i+1} = \alpha_i \quad (i \text{ even}) \qquad \text{and} \qquad \dot{z}_{i+1} = (1+e)A\omega \cos(\theta)\cos(\alpha_i + \tau) - e\dot{z}_i. \quad (7a, b)$$

The state relations between impacts follow from equation (4) and are given by

$$\alpha_{i+1} = \alpha_{i+1}(\alpha_i, \dot{z}_i) \quad (i \text{ odd}) \qquad \text{and} \qquad \dot{z}_{i+1} = \dot{z}_i - g\sin(\theta)\left[\frac{\alpha_{i+1}-\alpha_i}{\omega}\right], \quad (8a, b)$$

where the formal equality $\alpha_{i+1} = \alpha_{i+1}(\alpha_i, \dot{z}_i)$ expresses the functional relationship between α_{i+1} and $(\alpha_i, \dot{z}_i)$. That an explicit form for this relationship does not exist follows by substituting expression (1) and the double integral of equation (4) into equation (2), and evaluating this at α_i and α_{i+1}. The resulting transcendental equation is given by

$$\Delta y_i + \dot{z}_i\left[\frac{\alpha_{i+1}-\alpha_i}{\omega}\right] - \tfrac{1}{2}g\sin(\theta)\left[\frac{\alpha_{i+1}-\alpha_i}{\omega}\right]^2 + A\cos(\theta)[\sin(\alpha_i+\tau) - \sin(\alpha_{i+1}+\tau)] = 0, \quad (9)$$

where $\Delta y_i = y_i - y_{i+1}$.

Equations (7) and (8) along with the relation (9) completely characterize the transient and periodic motions of m. Because of the implicit nature of equation (8a), however, these equations do not provide a straightforward means of determining the existence of steady state $K:L$ motions. The existence of such motions will instead be investigated by using constraint equations related to steady state solutions of the system. These constraint equations and a method for solving them are presented in the next section.

4. STEADY STATE SOLUTIONS AND THEIR STABILITY

Steady state periodic $K:L$ motions are characterized by

$$\alpha_{2K} = \alpha_0 + 2\pi L \qquad \text{and} \qquad \dot{Z}_{n+1} = \dot{z}_{2K} = \dot{z}_0 = \dot{Z}_n. \quad (10a, b)$$

Solutions of equations (10) for some $\{\alpha_i\}_{i=2(i\text{ even})}^{2K-2}$ and τ are sufficient for the existence of assumed $K:L$ motions. Specifically, equations (7b) and (8b) can be used to find explicit expressions for $\dot{z}_i$, $i = 0, 1, \ldots, 2K-1$, as functions of $\{\alpha_i\}_{i=2\ (i\text{ even})}^{2K-2}$ and τ. These expressions and expression (7a) when substituted into equation (9), form K constraint equations with the K unknowns $\{\alpha_i\}_{i=2\ (i\text{ even})}^{i=2K-2}$ and τ. If the constraint (9) relates (a) two consecutive impacts on the same side of M, then $\Delta y_i(d) = 0$, or (b) a left to right impact sequence, then $\Delta y_i(d) = -d$, or (c) a right to left impact sequence, then $\Delta y_i(d) = d$.

The K equations generated from equation (9) can be used to solve for the K unknowns $(\{\alpha_i\}_{i=2\ (i\text{ even})}^{2K-2}, \tau)$ which will be denoted by $(\bar{\alpha}, \bar{\tau})$. From equations (7b) and (8b) it is clear that $(\bar{\alpha}, \bar{\tau})$ uniquely determines the $\bar{z}_i$'s, so that $(\bar{\alpha}, \bar{\tau})$ represents a steady state $K:L$ motion of the inclined impact pair.

Solutions of equation (9) must also satisfy the additional constraint

$$|y(\alpha)| = |z(\alpha) - x(\alpha)\cos(\theta)| \leqslant d/2. \quad (11)$$

Such solutions $(\bar{\alpha}, \bar{\tau})$ which violate this constraint are physically impossible, and have been called non-viable solutions [7, 8]. Note that this constraint is on the entire motion, and can be checked only after the possible steady state motions have been determined.

To study the local stability of a $K:L$ motion represented by $(\bar{\alpha}, \bar{\tau})$, the fixed point $(T_n, \dot{Z}_n) = (\alpha_0, \dot{z}_0)$ in equation (6) is perturbed a small amount $(\Delta T_n, \Delta \dot{Z}_n) = (\xi_0, \eta_0)$ to give

$$(\Delta T_{n+1}, \Delta \dot{Z}_{n+1}) = DP(\Delta T_u, \Delta \dot{Z}_n) + G(\Delta T_n, \Delta \dot{Z}_n). \tag{12}$$

Here, DP is the Jacobian of P evaluated at $(\bar{\alpha}, \bar{\tau})$, and $G(\cdot)$ is a function of the non-linear terms of the Taylor series expansion of equation (6) about $(T_n, \dot{Z}_n)$. Substituting

$$\alpha_i = \bar{\alpha}_i + \xi_i \qquad \text{and} \qquad \dot{z}_i = \bar{\dot{z}}_i + \eta_i \tag{13a, b}$$

into equations (6), (7b), and (8) yields the general non-linear difference equations

$$\begin{bmatrix} \xi_{i+1} \\ \eta_{i+1} \end{bmatrix} = DP^{(i)} \begin{bmatrix} \xi_i \\ \eta_i \end{bmatrix} + \begin{bmatrix} f(\xi_i, \eta_i) \\ g(\xi_i, \eta_i) \end{bmatrix}, \tag{14a}$$

where

$$DP^{(i)} = \begin{bmatrix} \partial\alpha_{i+1}/\partial\alpha_i & \partial\alpha_{i+1}/\partial\dot{z}_i \\ \partial\dot{z}_{i+1}/\partial\alpha_i & \partial\dot{z}_{i+1}/\partial\dot{z}_i \end{bmatrix}_{(\bar{\alpha}, \bar{\tau})} \tag{14b}$$

and the functions f and g contain the non-linear perturbation terms. Sequentially combining the $2K$ equations resulting from equations (14) gives

$$\begin{bmatrix} \xi_{2K} \\ \eta_{2K} \end{bmatrix} = DP \begin{bmatrix} \xi_0 \\ \eta_0 \end{bmatrix} + \begin{bmatrix} f(\xi_0, \eta_0 \\ g(\xi_0, \eta_0) \end{bmatrix}, \tag{15a}$$

where

$$DP = \begin{bmatrix} \partial\alpha_{2K}/\partial\alpha_0 & \partial\alpha_{2K}/\partial\dot{z}_0 \\ \partial\dot{z}_{2K}/\partial\alpha_0 & \partial\dot{z}_{2K}/\partial\dot{z}_0 \end{bmatrix}_{(\bar{\alpha}, \bar{\tau})} = DP^{(2K-1)} \cdots DP^{(1)} DP^{(0)} \tag{15b}$$

is the Jacobian of P. Since the perturbation variables are assumed to be small, the non-linear terms in equation (15a) can usually be ignored when discussing the local stability of the motion. It is well known [15, 17] that the $K:L$ motion will be stable if the eigenvalues of DP satisfy $|\lambda_i| < 1$, $i = 1, 2$. In the case that one of the eigenvalues lies on the unit circle, the stability of the $K:L$ motion depends upon the non-linear terms in equation (14a). These equations related to the stability of $K:L$ motions are now developed.

The Jacobian matrix DP can be calculated from equation (15b). To this end, first note that the elements of the matrices $DP^{(i)}$, calculated by implicit differentiation of equation (7), for i even are

$$\partial\alpha_{i+1}/\partial\alpha_i = 1, \qquad \partial\alpha_{i+1}/\partial\dot{z}_i = 0, \tag{16a, b}$$

$$\partial\dot{z}_{i+1}/\partial\alpha_i = -(1+e)A\omega \cos(\theta) \sin(\alpha_i + \tau), \qquad \text{and} \qquad \partial\dot{z}_{i+1}/\partial\dot{z}_i = -e. \tag{16c, d}$$

Similarly, for i odd equation (8) yields

$$\frac{\partial\alpha_{i+1}}{\partial\alpha_i} = \left\{ \frac{\dot{z}_i}{A\omega \cos(\theta)} - \frac{g(\alpha_{i+1} - \alpha_i) \tan(\theta)}{A\omega^2} - \cos(\alpha_i + \tau) \right\} \Big/ D_i \tag{17a}$$

$$\partial\alpha_{i+1}/\partial\dot{z}_i = -(\alpha_{i+1} - \alpha_i)/A\omega \cos(\theta) D_i, \tag{17b}$$

$$\frac{\partial\dot{z}_{i+1}}{\partial\alpha_i} = \frac{-g[\cos(\alpha_{i+1} + \tau) - \cos(\alpha_i + \tau)] \sin(\theta)}{\omega D_i}, \tag{17c}$$

$$\frac{\partial\dot{z}_{i+1}}{\partial\dot{z}_i} = \left\{ \frac{\dot{z}_i}{A\omega \cos(\theta)} - \cos(\alpha_{i+1} + \tau) \right\} \Big/ D_i \tag{17d}$$

where

$$D_i = \frac{\dot{z}_i}{A\omega \cos(\theta)} - \frac{g(\alpha_{i+1} - \alpha_i)\tan(\theta)}{A\omega^2} - \cos(\alpha_{i+1} + \tau).$$

With some effort, it can be shown that

$$\text{Det}[DP^{(i)}] = -e, \qquad i = 0, 2, \ldots, 2K-2. \tag{18a}$$

Substitution of equations (2) and (8) into equations (17) yields

$$\text{Det}[DP^{(i)}] = \dot{y}_i / \dot{y}_{i+1}, \qquad i = 1, 3, \ldots, 2K-1. \tag{18b}$$

Finally, equations (3), (15b), and (18) along with the chain rule give

$$\text{Det}[DP] = (-e)^K \frac{\dot{y}_1 \dot{y}_3 \cdots \dot{y}_{2K-1}}{\dot{y}_2 \dot{y}_4 \cdots \dot{y}_{2K}} = (-e)^K \frac{\dot{y}_1 \dot{y}_3 \cdots \dot{y}_{2K-1}}{\dot{y}_0 \dot{y}_2 \cdots \dot{y}_{2K-2}} = e^{2K}. \tag{19}$$

Since only $e < 1$ cases are considered, $\text{Det}[DP] = \lambda_1 \lambda_2 = e^{2K} < 1$. Thus, if the eigenvalues are complex, they they form a complex conjugate pair lying on a circle of radius $e^K < 1$. If they are assumed to be initially complex for a given set of system parameters, then the only way instability can occur via variation of a specified parameter is for λ_1 and $\lambda_2 = \bar{\lambda}_1$ to merge on the real axis at $\pm e^K$ and then split, one going toward the origin and the other going toward $\pm\infty$. Specifically, the only way for the motion to become unstable is for the critical eigenvalue to pass through the unit circle on the real axis.

Even though it is not possible to obtain a general expression for the trace $\text{Tr}[DP]$ of DP, once the number of impacts is known, it can be determined by using equations (14b), (15), (16), and (17). The eigenvalues of DP can then be calculated directly from the equation

$$\lambda_{1,2} = \tfrac{1}{2}\left[-\text{Tr}[DP] \pm \sqrt{\text{Tr}[DP]^2 - 4e^{2K}} \right]. \tag{20}$$

To summarize the procedure for determining the existence and stability of an assumed $K:L$ motion, first equations (6b) and (7b) are used to find explicit expressions for the $\dot{z}_i$'s as functions of the α_i's and τ. Then, based on the type of impact sequence assumed, equation (9) is used to generate the K constraint equations. Solutions $(\bar{\alpha}, \bar{\tau})$ of these equations, if they exist, define steady state $K:L$ motions. After having checked the viability condition (11), the local stability of each of these motions is then determined by the eigenvalues of the Jacobian matrix DP, evaluated at $(\bar{\alpha}, \bar{\tau})$. If $|\lambda_i| < 1$, $i = 1, 2$, the motion is stable. Finally, it should be noted that once a $K:L$ motion is specified, the general expressions generated for the $\dot{z}_i$'s and the stability equations are fixed, regardless of what type of impact sequence is chosen.

5. BIFURCATION ANALYSIS

Before presenting some numerical results for some specific $K:L$ motions we give a brief summary of the bifurcation analysis which was used to predict existence boundaries, as well as new stable motions which may result when an assumed steady state motion becomes unstable. Stable steady state motions may become unstable as the system parameters are changed, and new motions may be created at that point via bifurcations. The type of new, or bifurcating motion will depend upon the type of bifurcation that occurs, and its stability will depend on whether the bifurcation is supercritical or subcritical. The new motion is stable if the bifurcation is supercritical.

The discussion here will be limited to co-dimension one bifurcations; that is, bifurcations that typically occur when only one of the system parameters is changed. Guckenheimer and Holmes [16] have listed several types of bifurcations. The type of bifurcation which occurs depends on the sign of the critical eigenvalue λ_c, and on the lowest order non-linear terms of the Taylor series expansion of the return map, P, at the bifurcation point. For $\lambda_c = +1$ one of three types of bifurcations can occur. The first is a saddle node bifurcation, which occurs when a stable and an unstable solution branch merge and annihilate each other. This point represents a solution existence boundary in the parameter space. The second is a pitchfork bifurcation, in which a symmetric stable solution branch becomes unstable, and in doing so generates two new non-symmetric solution branches. The third is a transcritical bifurcation. It occurs when two solution branches having opposite stability characteristics cross and exchange stability characteristics. The new solution branches created by the pitchfork and transcritical bifurcations have the same period as the original solutions.

For $\lambda_c = -1$, only a period doubling bifurcation can occur. In this case, the new steady state motion has twice the period of the old one. Another type of bifurcation, called the Hopf bifurcation, occurs when a pair of complex eigenvalues exits the unit circle as a complex conjugate pair. This type of bifurcation cannot occur in the inclined impact pair because the product of the eigenvalues has already been shown to satisfy $\lambda_1\lambda_2 = e^{2K} < 1$.

6. NUMERICAL RESULTS

In this section some numerical results, in the form of stability plots, are presented in order to gain a better understanding of the system dynamics for a variety of motions and parameter combinations. Results are presented for 1:1, 2:1 and 3:1 motions. The constraint equations governing these motions are contained in the Appendix, wherein the development for $1:L$, $2:L$ and 3:1 motions is presented in detail. In addition to this development some simple consequences are also discussed there. For example, it is shown that equispaced 2:1 motions cannot be supported for non-zero angles of inclination. Here, we first quantify some results obtained for the 1:1 motion. Results for 2:1 motion are only summarized here, since they are discussed more fully in reference [15]. They are repeated primarily to demonstrate the utility of the equations developed, and to emphasize their relationship to other motions. Finally, some results related to the 3:1 motions are presented in section 7.3. The emphasis here will be on some complex bifurcation behavior observed for these motions in a small interval of inclination angle, θ, around 35°.

6.1. 1:1 MOTIONS

A typical 1:1 motion is shown in Figure 2. The stability regions in the γ-θ plane for $e = 0{\cdot}1$, $0{\cdot}5$, $0{\cdot}9$ are shown in Figure 3. The lower stability boundaries governed by equation (A3) are shown by solid lines. They indicate the occurrence of saddle node bifurcations, where two solutions having opposite stability characteristics arise. As such, they are also existence boundaries. The upper stability boundaries defined by equation (A6) are the dashed lines. These show where flip bifurcations occur. As expected from equations (A3) and (A6), the range of γ values which can support stable 1:1 motion decreases with decreasing inclination angle θ and with increasing energy dissipation (decreasing e).

Figure 4 shows a typical stability region for 1:1 motion in the ρ-θ plane. The solid and dashed lines, which indicate the same stability characteristics as those in Figure 3, are vertical as a consequence of their independence of ρ. The effect of ρ is seen as the

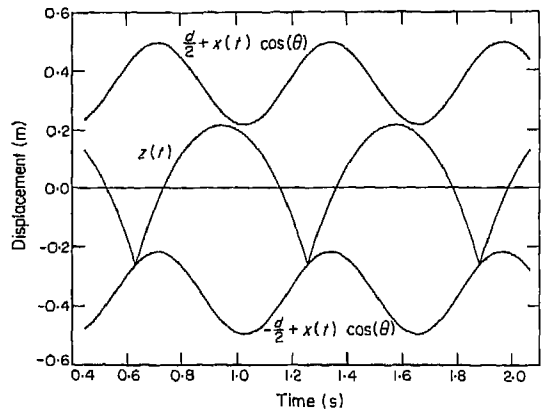

Figure 2. A 1:1 motion; $\rho = 2{\cdot}8$, $\theta = 82°$, $\gamma = 10{\cdot}2$, $e = 0{\cdot}5$.

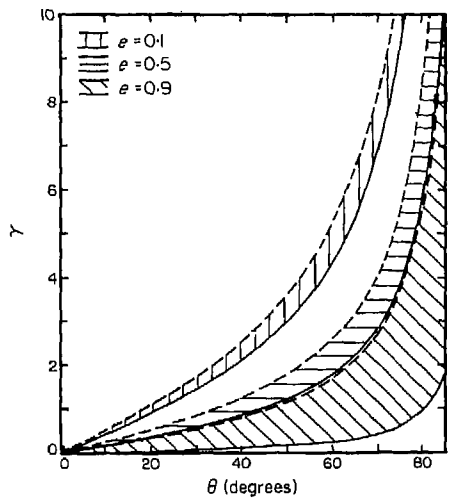

Figure 3. Stability zones of 1:1 motion in the γ–θ plane.

thick line at the top of the shaded region, which represents a viability boundary [cf equation (11)]. When a 1:1 motion passes through a viability boundary the new stable motion, if there is one, cannot be predicted by the bifurcation analysis of the last section. The range of θ values for this shaded region may be computed by using equation (A5) and (A7), with $\mathrm{Tr}\,[DP] = \pm(1+e^2)$.

Several general features which verify the analysis in the Appendix can be extracted from Figures 3 and 4. For small accelerations γ no 1:1 motions exist. This is because the secondary mass m cannot attain the initial velocities necessary to stay up for one cycle of the primary mass. The minimum value of γ for which 1:1 motions exist increases with increasing inclination angle θ and energy dissipation. As γ is increased, or θ is decreased, the 1:1 motions become unstable and new 2:2 motions are created via a flip or period doubling bifurcation. Simulations and the bifurcation analysis outlined in section 5 confirmed that close to this stability boundary the new 2:2 motions are stable.

Figure 5 represents a chaotic motion resulting from the iterates of the map (6) for θ values beyond the period-doubling cascade of 1:1 motions. The motion shown represents 20 000 impacts, all of which occur on the left end. This motion is aperiodic, and

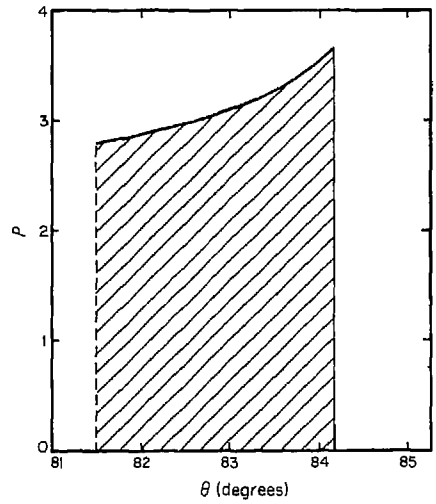

Figure 4. Stability zone of 1:1 motion in the ρ–θ plane; $\gamma = 10{\cdot}2$.

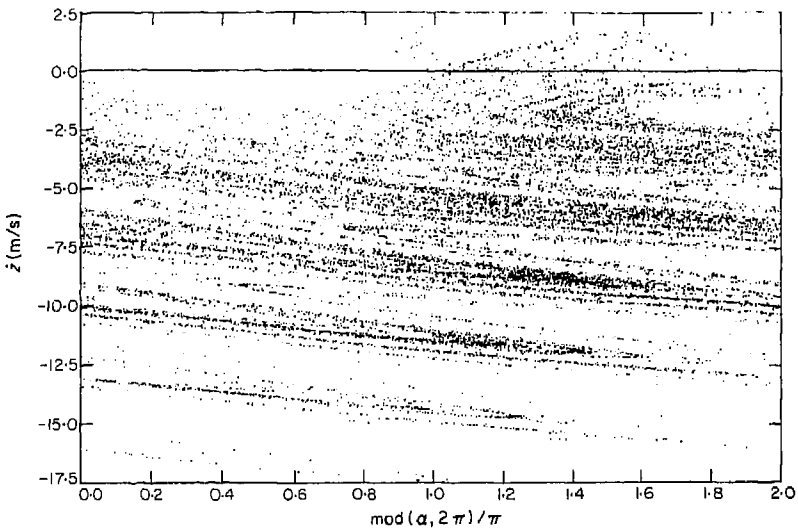

Figure 5. Chaotic solutions of the map found beyond the 1:1 period doubling bifurcation cascade; $\rho = 0{\cdot}01$, $\theta = 80°$, $\gamma = 10{\cdot}2$, $e = 0{\cdot}9$.

characterizes a strange attractor which is weak in the sense that the motion tends to wander almost uniformly over the state space region shown. In this respect, it differs from the results presented by Holmes in reference [9], suggesting that the angle of inclination affects the strange attractor in an essential way.

6.2. 2:1 MOTIONS

The numerical results for 2:1 motions have already been discussed in reference [15], so that only a few representative results will be presented here. Examples of 2:1 motions are shown in Figure 6. Figures 6(a) and 6(b) show a stable $\alpha > \pi$ motion and a stable $\alpha < \pi$ motion existing at the same value of $\rho = 1{\cdot}0$. Increasing ρ to a value $\rho = 1{\cdot}18$ yields Figure 6(c), which represents a grazing impact where the motion is on the verge of

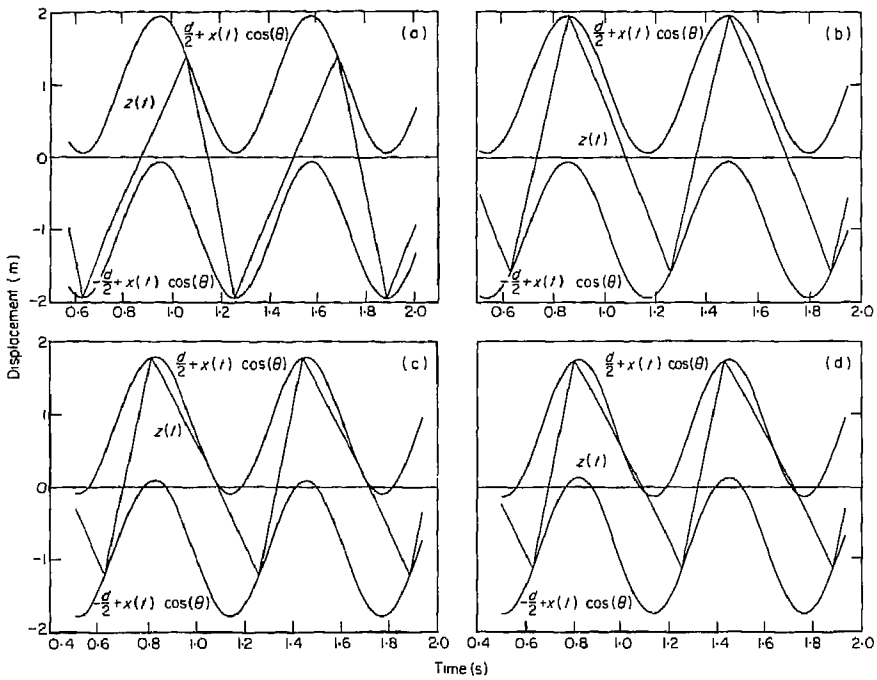

Figure 6. 2:1 Motions. (a) Stable, viable $\alpha > \pi$; $\rho = 1{\cdot}0$, $\theta = 20°$, $\gamma = 10{\cdot}2$, $e = 0{\cdot}5$; (b) stable, viable $\alpha < \pi$; $\rho = 1{\cdot}0$, $\theta = 20°$, $\gamma = 10{\cdot}2$, $e = 0{\cdot}5$; (c) stable motion on the viability boundary; $\rho \approx 1{\cdot}18$, $\theta = 20°$, (d) non-viable motion; $\rho = 1{\cdot}22$, $\theta = 20°$, $\gamma = 10{\cdot}2$, $e = 0{\cdot}5$.

violating condition (11). *Figure* 6(*d*) *represents a non-viable motion, obtained when* ρ exceeds the value corresponding to a grazing impact. It is clear that m penetrates M between the second and third impact.

A typical stability plot for 2:1 motion in the ρ–θ plane is shown in Figure 7. The value of $e = 0{\cdot}5$ was chosen to illustrate the effects of viability boundaries, which are absent for higher values of e. There are two distinct stability zones, one for $\alpha > \pi$ motions and

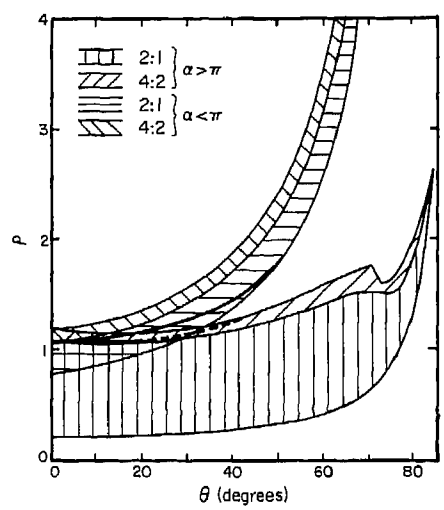

Figure 7. Stability zones of 2:1 motion and 4:2 motion for $\gamma = 10{\cdot}2$ and $e = 0{\cdot}5$.

a second for $\alpha < \pi$ motions. The lower stability boundary for both motions corresponds to a saddle node bifurcation ($\lambda_c = +1$). No stable or unstable 2:1 motions exist below this boundary. The upper stability boundary corresponds to a period doubling bifurcation ($\lambda_c = -1$), at which point 4:2 motions are created. The stability plots for 4:2 motions are also shown in this figure. The thick solid and dashed lines represent viability boundaries for the motion type in which they are found. No solutions of the appropriate type are physically meaningful above these boundaries. Stable non-viable solutions are shown here in order to emphasize the role played by the viability condition. Figure 7 also shows that both $\alpha > \pi$ and $\alpha < \pi$ stable motions can co-exist for a range of parameters ρ and θ.

As shown by equation (A12) and mentioned earlier, equispaced motions exist only if $\theta = 0$. The lower stability boundary for equispaced motions also corresponds to a saddle node bifurcation. As ρ is increased the stable equispaced motion eventually becomes unstable via a pitchfork bifurcation ($\lambda_c = +1$). New stable 2:1 $\alpha > \pi$ motion is created by this bifurcation. Increasing ρ further results in this new motion becoming unstable via period doubling bifurcations ($\lambda_c = -1$).

The extent of the stability regions and the viability of solutions are greatly influenced by the system parameters e and γ. These effects can be summarized as follows (see reference [15] for details). For fixed acceleration γ, increasing e allows stable 2:1 motions to exist for larger inclination angles, θ, and slot lengths, d. Overlapping stability regions for $\alpha > \pi$ and $\alpha < \pi$ motions also increase with e. Finally, increasing e tends to increase the viability of a 2:1 motion. For $e \geq 0{\cdot}9$ no viability boundary appears in the stable 2:1 and 4:2 regions.

As γ is reduced the stability regions in the ρ–θ plane are reduced, in that stable 2:1 motions exist for smaller inclination angles θ. In some cases with small e, no 2:1 $\alpha < \pi$ motions exist when $\theta > 0$. Increasing γ tends to negate the effects of gravity so that stable 2:1 motions are found for larger θ. In addition, regions of co-existence of the two types of stable 2:1 motions increase, as do the regions of viable motions.

For large e, where the viability is not a factor, increasing ρ may result in the motion of m going through a cascade of period doubling bifurcations, until the motion eventually

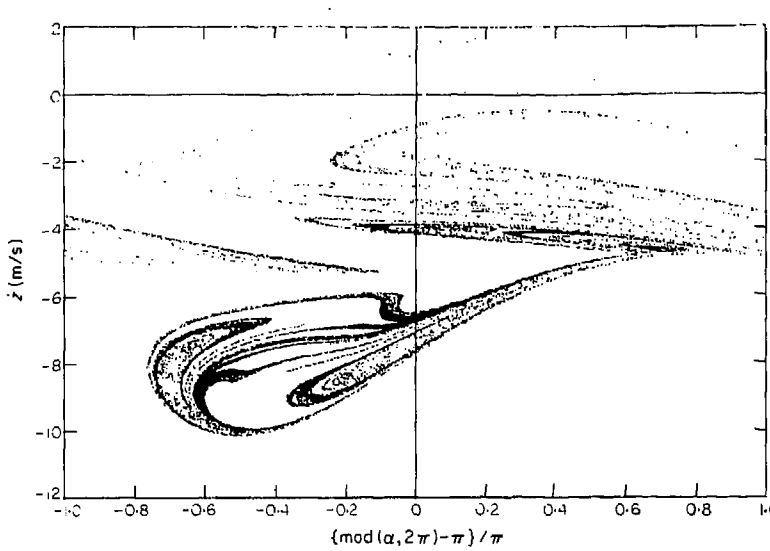

Figure 8. Chaotic solutions of the map found above the 2:1 period doubling bifurcation cascade; $\rho = 1{\cdot}39$, $\theta = 80°$, $\gamma = 10{\cdot}2$, $e = 0{\cdot}9$.

becomes chaotic. A steady state solution resulting from the iterates of the map (6) in the $[\alpha, \dot{z}]$ phase plane is shown in Figure 8. The motion shown represents 40 000 impacts, of which 23 106 impacts occurred on the left side. The motion is aperiodic, but is bounded and appears to be attracted to certain regions in the phase space, as opposed to the chaotic motion in Figure 5. This attractive set is the so-called strange attractor [15, 18]. The very dense regions inside the strange attractor are located near unstable manifolds of the 2:1, 4:2, and other subharmonic motions. If a cylinder is formed out of Figure 8 it is easy to see that the strange attractor is periodic with respect to α.

6.3. 3:1 MOTIONS

In simulations for 2:1 motions it was noted that stable 3:1 motions typically resulted when 2:1 motions became non-viable. Such motions also represent the simplest class of necessarily non-symmetric $K:L$ motions. There are two possible types of 3:1 steady state motions for impacts occuring at both ends of the slot. The first includes two impacts on the left side before an impact on the right. We call this a LLR sequence. The second consists of one impact on the left followed by two impacts on the right. We call this a LRR sequence. Examples of these two types of 3:1 motion are illustrated in Figure 9. These motions are completely determined by α_I, α_{II}, and τ. Solutions for these parameters were obtained by using equation (A14) for a wide range of parameter values. Figures

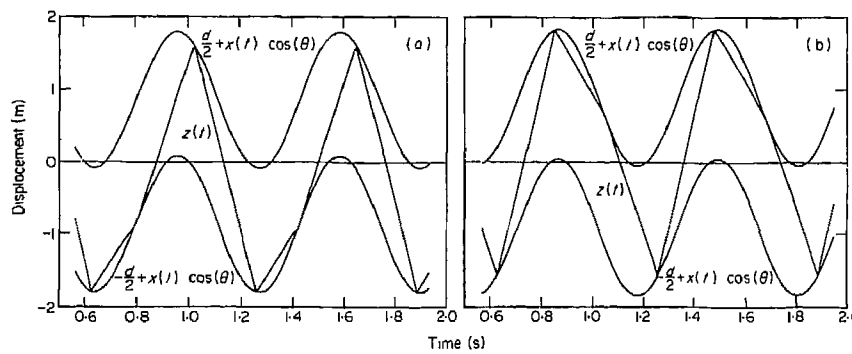

Figure 9. 3:1 Motions. (a) LLR; $\rho = 1{\cdot}17$, $\theta = 20°$, $\gamma = 10{\cdot}2$, $e = 0{\cdot}5$; (b) LRR; $\rho = 1{\cdot}12$, $\theta = 20°$, $\gamma = 10{\cdot}2$, $e = 0{\cdot}5$.

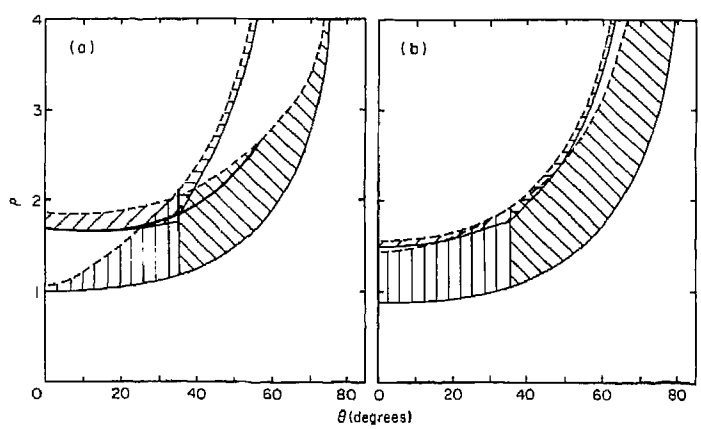

Figure 10. Stability zones of 3:1 LLR motion for $\gamma = 10{\cdot}2$. (a) $e = 0{\cdot}5$; (b) $e = 0{\cdot}9$.

10(a) and (b) show the stable regions of LLR motions for $e = 0{\cdot}5$ and $0{\cdot}9$, with $\gamma = 10{\cdot}2$. Figures 11(a) and (b) show the stable regions of LRR motions for the same parameters. Again, the solid line represents the boundary where a saddle node bifurcation occurs, and the dashed line represents the boundary where a period doubling bifurcation occurs. The thick solid line in Figure 10(a) is the viability boundary. As in the case of 1:1 and 2:1 motions, Figures 10 and 11 show that as e is increased the range of θ for which stable 3:1 motions exist is increased. Furthermore, the minimum value of ρ for which 3:1 motions exist is decreased.

The stability boundaries in Figure 10 appear to have discontinuities at $\theta \approx 35°$. These correspond to a very narrow transition zone where the upper existence boundary has a fold, and where stable and unstable solution branches are merging and splitting in a rather interesting manner. Figures 12(a-c) depict the qualitative behavior in this transition zone of small but non-zero width $\theta_l < \theta < \theta_r$. This width is approximately 0·5°. The thin solid and dashed curves indicate stability boundaries as in Figure 10. The thick solid and dashed curves are a qualitative representation of the stable and unstable solution branches, respectively.

Beginning in Figure 12(a), there are two solution branches to the left of θ_l. The solution branches which start at the lower saddle node bifurcation/stability boundary are designated as S_1, and those which start at the upper saddle node bifurcation/stability boundary are designated as S_2. These are further subscripted by s or u to reflect stable or unstable branches. On a saddle node stability boundary the solutions S_{is} are identical to S_{iu}, $i = 1$, 2, 3.

Figure 12(b) represents the solutions at θ_l. For a specific value of ρ the solution branches S_{1s} and S_{2u} touch. At this point the solutions of S_{1s} and S_{2u} are identical and have the same eigenvalues, one of which is +1. As ρ is increased further these branches split again.

Figure 12(c) represents the solutions in the transition zone (θ_l, θ_r). Here S_{1s} and S_{2u} merge at the crease portion of the fold in the second existence or saddle node bifurcation boundary. A new set of solutions, S_3, emerges from the upper portion of this second existence boundary. Clearly, S_{1s}, S_{2s}, and S_{2u} are really one solution branch with two different stable solutions for a small interval of ρ. An interesting consequence of the merging of S_{1s} and S_{2u} is the switching of the upper stability boundary for the S_{1s} solution. Its new upper stability boundary is the upper stability boundary for the S_{2s} solution. The upper stability boundary for the S_{3s} solution is the old upper stability boundary of the S_{1s} solution.

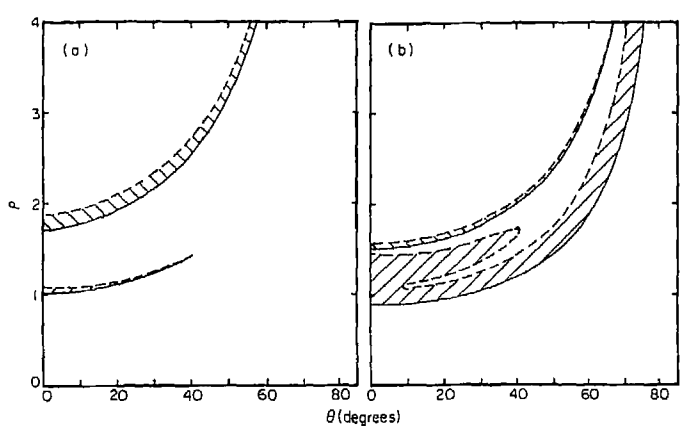

Figure 11. Stability zones of 3:1 LLR motion for $\gamma = 10{\cdot}2$. (a) $e = 0{\cdot}5$; (b) $e = 0{\cdot}9$.

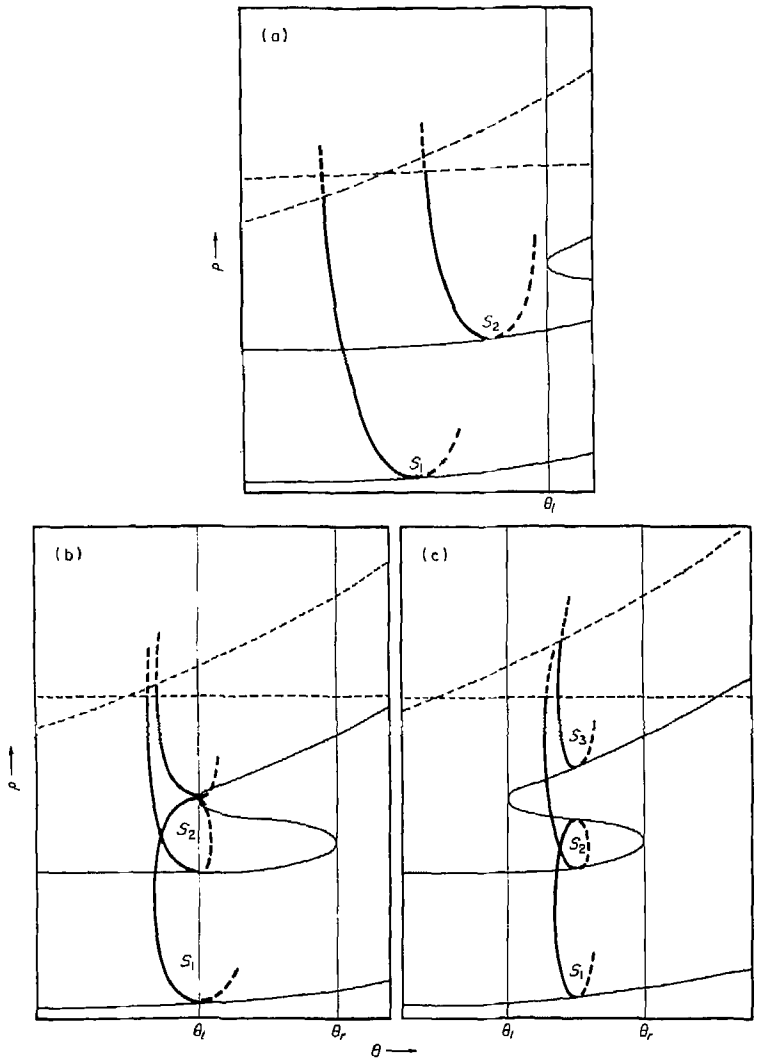

Figure 12. Qualitative representation of 3:1 LLR solution branches. (a) $\theta < \theta_1$, (b) $\theta = \theta_1$, (c) $\theta_1 < \theta < \theta_r$.

At $\theta = \theta_r$ the solution branch completely disappears and the S_{1s} and S_{2s} solutions merge to form one continuous solution brnach. For $\theta > \theta_r$ there are again only two solution branches.

From the above results it is clear that for the special values θ_l and θ_r of the inclination angle, multiple degeneracies arise in the solution of the constraint equations at some values ρ_l and ρ_r of the excitation amplitude. It is suspected that these points in the θ-ρ parameter plane correspond to singularities of co-dimension-two for the appropriate Poincaré mapping and a careful two-parameter unfolding analysis may reveal some interesting global dynamics.

The 3:1 motions show how complicated the dynamics of the inclined impact pair can become. There are some general conclusions regarding these motions which are similar to those for 1:1 and 2:1 motions. First, there are no 3:1 solutions for small values of ρ. Second, the minimum value of ρ for which 3:1 motions exist increases with increasing inclination angle, θ, and energy dissipation. Third, increasing ρ eventually results in 3:1

motions bifurcating into 6:2 motions. Simulations and the bifurcation analysis outlined in section 5 confirmed that the new 6:2 motions are stable. Fourth, for a given inclination angle, two stable 3:1 motions may co-exist at the same value of ρ. Generally, this only applies to LLR motions.

In addition, 3:1 motions exhibit some unique characteristics of their own. For example, one solution branch may have two different stable solutions for a small interval in ρ. In general, this result only applies to LLR sequences. The LRR motions are stable over a much smaller region in the ρ–θ plane. This can be expected because LRR motions impact twice at the top of the slot and gravity tends to prevent this, especially at large inclination angles. The LLR and LRR motions are stable over the same intervals of ρ when $\theta = 0$, and stable over different ranges of ρ for $\theta > 0$. Even so, the stability zones for the two motions tend to overlap for a wide range of ρ values. The area of overlap tends to increase with c. Although no stability charts for different values of γ are shown, one can infer from the 2:1 results and simulations of 3:1 motions that increasing γ results in an increase in the range of parameters for which stable motions exist. Even though, for small e, the stability charts for $\gamma = 10{\cdot}2$ are very different from those shown in Figure 10, most of the motion is non-viable, so that the differences are not physically meaningful.

The results found here for $\theta = 0°$ are not in complete agreement with those obtained by Bapat *et al.* [11], who showed a continuous set of solutions for a similar range of ρ. Our results show a gap between the two solution branches. Stable 3:1 solutions, both as solutions of the constraint equations and via simulations, were not found in this gap. There are at least two possible explanations for this discrepancy. One is that the method of finding solutions in reference [11] allows for some error, so that some of the solutions may not really exist as exact solutions of equation (A14). The other but less likely possibility is that we may not have found the correct initial conditions to give to ZSCNT to converge to the stable solutions.

So far, we have described the results for specific types of steady state motions assumed in the analysis of the inclined impact pair. These results are summarized in the following to form a more coherent picture of the dynamics of the system.

6.4. SUMMARY OF NUMERICAL RESULTS

An existing $K:L$ motion is usually stable over a finite interval of the parameter ρ representing the amplitude of the base motion. The lower stability boundary corresponds to an existence boundary where a saddle node bifurcation occurs. In general, the upper stability boundary corresponds to a period doubling or flip bifurcation where new stable period doubled motions are created. Only for $\theta = 0$ is the period doubling bifurcation preceded by a pitchfork bifurcation, which occurs when the equispaced 2:1 motions become unstable and bifurcate into non-equispaced 2:1 motions. For 3:1 motions, the exception is the narrow transition zone near 35° where a saddle node bifurcation occurs. In any case, the new motion eventually experiences a period doubling bifurcation. The period doubling process continues, leading ultimately to chaotic motions unless terminated by a viability boundary. Transcritical bifurcations never occurred for the motions studied.

The viability boundary is prominent for low values of the coefficient of restitution, e, and small accelerations, γ. For large γ and large $e < 1$, the bifurcation cascade ultimately results in aperiodic, or chaotic motions of the small mass.

The coefficient of restitution, e, which provides the only energy dissipation mechanism within the system, has many effects upon the motion. In general, increasing e raises the maximum value of inclination θ, and reduces the minimum value of ρ for which a particular $K:L$ motion exists. The viability boundary is greatly affected by e; so much that it disappears when e is large.

Even though these results were obtained for no viscous damping in the slot, the inclusion of small amounts of such a retarding force would be expected only slightly to modify these results. In particular, one might expect that the reduced velocity of m in its motion through the slot would be compensated for by slightly greater impact velocities resulting from a changed value of phase τ.

The acceleration γ also plays an important role in the dynamics of the system. Increasing γ raises the maximum value of θ for which a particular $K:L$ motion exists, as well as the maximum value of ρ for which the motion is viable.

As stated earlier, the motion of m is dependent upon the system parameters and the initial conditions $(\tau, \dot{z}_0)$. Earlier it was shown that stable $\alpha > \pi$ and $\alpha < \pi$ 2:1 motions can exist for the same parameter set. A similar observation is made for the 3:1 motions. It is also possible that more than one type of stable $K:L$ motions exist for the same parameter set. For example, Figure 13 shows the stability regions for viable 1:1, 2:1, and 3:1 LLR motions for $e = 0{\cdot}5$ and $\gamma = 10{\cdot}2$. The overlap of stability regions of the various stable motions is expected to increase with the coefficient of restitution e and acceleration γ. Thus, there are parameter values for which more than one type of steady state motions are stable. The actual motion observed in long-time simulations or in experiments then depends on initial conditions and the domains of attraction in the state space of the various solutions.

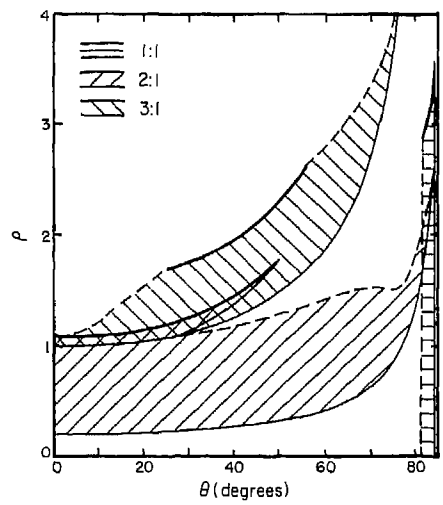

Figure 13. Stability of 1:1, 2:1, and 3:1 LLR motions; $\gamma = 10{\cdot}2$, $e = 0{\cdot}5$.

A more striking example of the coexistence of various stable motions for the same values of parameters is shown in Figure 14 and Figure 15. Figure 14 shows a chaotic solution of the Poincaré map for parameter values given by $\rho = 0{\cdot}22$, $\theta = 80°$, $\gamma = 10{\cdot}2$, and $e = 0{\cdot}9$. The initial conditions for the transient motion are $\tau \approx 84{\cdot}7°$ and $\dot{z}_0 \approx -3{\cdot}03$ m/s. Figure 15 shows a stable 2:1 motion which exists for the same values of the parameters. The initial conditions for the stable 2:1 motion are $\tau \approx -26{\cdot}8°$ and $\dot{z}_0 \approx -31{\cdot}0$ m/s. It is apparent from Figure 14 that, even after 20 000 impacts (18 830 on the left end), the velocity required for periodic 2:1 motion is never reached. Therefore, it is doubtful that the motion will ever stabilize into the 2:1 motion shown in Figure 15.

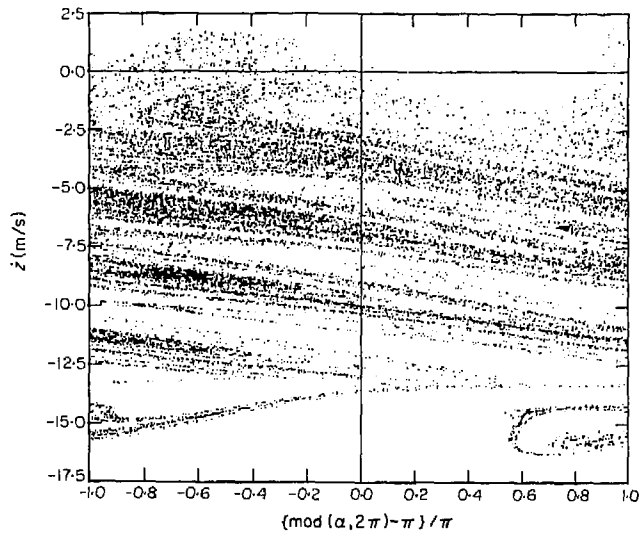

Figure 14. Chaotic solutions of the map existing in stable 2:1 region; $\rho = 0{\cdot}22$, $\theta = 80°$, $\gamma = 10{\cdot}2$, $e = 0{\cdot}9$.

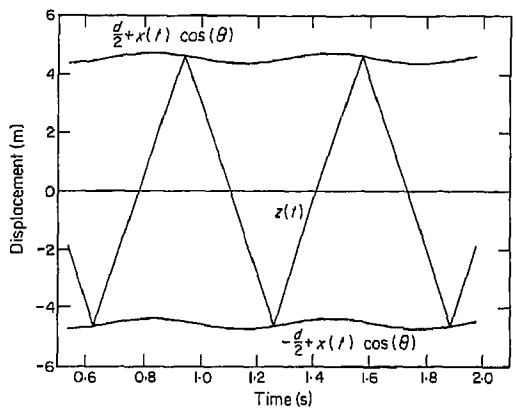

Figure 15. A stable 2:1 $\alpha > \pi$ motion; $\rho = 0{\cdot}22$, $\theta = 80°$, $\gamma = 10{\cdot}2$, $e = 0{\cdot}9$.

7. NON-VIABLE MOTIONS

In the development so far, it has been seen that sometimes the solutions of the constraint equations (7) for an assumed $K:L$ motion result in physically impossible or non-viable motions. Non-viable motions of the inclined impact pair are those solutions of equations (7) for which the secondary mass m must penetrate one of the walls of the slot in order to accomodate a given $K:L$ motion. These solutions have no physical meaning and care should be taken to avoid them. In previous works [4–8], non-viable motions were eliminated by enforcing condition (11) via simulating the motion and visually checking it. This method is accceptable if just a few solutions are to be checked, but is very inefficient if used to find the boundaries in the parameter plane at which motions become non-viable. Here, we develop an algorithm for determining the viability boundaries for a given $K:L$ motion with respect to one of the system parameters ρ, e, θ, or γ. First, however, we present some preliminary results obtained in reference [15] in order to understand how motions become non-viable, and the unique characteristics associated with motions on a viability boundary.

Figure 6 shows how a stable, viable 2:1 motion changes as the length of the slot is decreased, or ρ is increased. Figure 6(b) shows a stable, viable 2:1 motion. Note that the motion of the secondary mass m remains bounded by the walls of the slot between impacts. The motion shown in Figure 6(c) is also a stable, viable 2:1 motion. However, the upper end of the slot catches up with the mass just after impact between the second and third impacts, so that the relative displacement between the two masses is $d/2$ and the relative velocity is zero. The impact depicted here has been called a grazing impact because, although the masses touch, there is no instantaneous change in velocity at impact. This type of motion defines the viability boundary. Figure 6(c) shows a non-viable motion in which the mass m penetrates the upper end of the slot between the "expected" impacts.

As shown above, the viability boundary corresponds to the parameter value for which a grazing impact occurs for a given $K:L$ motion. This impact will occur at some time α_v where $\alpha_i < \alpha_v < \alpha_{i+1}$ (i odd), so that

$$|y(\alpha_v)| = d/2 \qquad \text{and} \qquad \dot{y}(\alpha_v) = 0. \tag{21a, b}$$

Equations (21) provide two additional constraint equations which can be used to find a viability boundary. The constraint (21a) is formed by replacing α_{i+1} with α_v in equation (7). The constraint (21b) is simply the first derivative of equation (2) with respect to time evaluated at α_v. Equations (7) and (21) give $K+2$ constraint equations with the $K+2$ unknowns $\{\alpha_i\}_{i=2\ (i\ \text{even})}^{2K-2}$, α_v, τ, and another unknown which can be chosen from one of the system parameters ρ, γ, θ, or e. If ρ is chosen as the parameter of interest, the $K+2$ constraint equations can be solved numerically to find ρ_v, which defines the viability boundary. For any value of $\rho > \rho_v$ the motion is non-viable. In general, the state i, which is used with equations (21) as an initial condition, must be found via simulations. The viability boundaries shown in this work were determined by using this approach, and were verified via simulations.

8. SUMMARY AND CONCLUSIONS

The dynamics of a frictionless inclined impact pair has been studied. The motion of the small mass was studied via the concept of a return map. Although an explicit expression for the map is unobtainable, it was possible to derive constraint equations which enforced the desired motion. The K non-linear constraint equations were derived directly from relationships which were implicit functions of the map. These constraint equations were used to show the existence and viability of specified $K:L$ motions. Perturbations of the appropriate maps were used to study the stability and subsequent bifurcations of the motions. Equations for $1:L$, $2:L$, and 3:1 motions were derived and analysis for $L=1$ motions was carried out.

Several results were obtained directly from the theoretical analysis. A new algorithm was developed for finding the viability boundary of a $K:L$ motion. This is signifiant since it obviates the need for running simulations of the motion to check for their viability. The stability analysis showed that $\text{Det}[DP] = \lambda_1\lambda_2 = e^{2K} < 1$. The major consequence of this is that the eigenvalues can exit the unit cycle only on the real axis (i.e., $\lambda_c = \pm 1$). This makes it impossible for Hopf bifurcations to occur in the inclined impact pair. The relation $\text{Det}[DP] = e^{2K} < 1$ for $e < 1$ seems to be a common characteristic of impacting mechanical systems (cf. [7-10]). It was shown that equispaced motions do not exist for $\theta \neq 0$. Thus, in an experimental investigation of the "horizontal" impact pair it may not be possible to detect equispaced motions due to inherent small inclinations.

Numerical results showed that the coefficient of restitution e and the acceleration γ have significant influence on the stability regions in the ρ-θ plane. In general, large e

and γ increase the viability of stable motions. Multiple stable steady state motions can coexist for a given parameter set. The actual motion depends on the initial conditions. In cases where viability does not interfere, the steady state motions undergo period doubling bifurcations with increasing ρ, and ultimately lead to chaotic motions.

REFERENCES

1. C. GRUBIN 1956 *Journal of Applied Mechanics* **78**, 373–378. On the theory of the acceleration damper.
2. S. F. MASRI and T. K. CAUGHEY 1966 *Journal of Applied Mechanics* **33**, 586–592. On the stability of the impact damper.
3. C. N. BAPAT and S. SANKAR 1985 *Journal of Sound and Vibration* **99**, 85–94. Single unit impact damper in free and forced vibration.
4. M. M. SADEK and B. MILLS 1970 *Journal of Mechanical Engineering Science* **12**, 268–277. Effect of gravity on the performance of an impact damper, part 1: Steady state motion.
5. M. M. SADEK and C. J. H. WILLIAMS 1970 *Journal of Mechanical Engineering Science* **12**, 278–287. Effect of gravity on the performance of an impact damper, part 2: stability of vibrational modes.
6. M. SENATOR 1970 *Journal of the Acoustical Society of America* **47**, 1390–1397. Existence and stability of periodic motions of a harmonically forced impacting system.
7. S. W. SHAW and P. J. HOLMES 1983 *Journal of Sound and Vibration* **90**, 129–155. A periodically forced piecewise linear oscillator.
8. S. W. SHAW 1985 *Journal of Applied Mechanics* **52**, 453–464. The dynamics of a harmonically excited system having rigid constraints, part 1: Subharmonic motions and local bifurcations; part 2: Chaotic motions and global bifurcations.
9. P. J. HOLMES 1982 *Journal of Sound and Vibration* **84**, 173–189. The dynamics of repeated impact with a sinusoidally vibrating table.
10. R. M. EVERSON, 1986 *Physica* **19D**, 355–383. Chaotic dynamics of a bouncing ball.
11. C. N. BAPAT, N. POPPLEWELL, and K. MCLACHLAN 1983 *Journal of Sound and Vibration* **87**, 19–40. Stable periodic motions of an impact-pair.
12. M. A. VELUSWAMI and F. R. E. CROSSLEY 1975 *Journal of Engineering for Industry* **97**, 820–827. Multiple impacts of a ball between two plates, part 1: some experimental observations.
13. M. A. VELUSWAMI, F. R. E. CROSSLEY, and G. HORVEY 1975 *Journal of Engineering for Industry* **97**, 828–835. Multiple impacts of a ball between two plates, part 2: mathematical modelling.
14. A. B. PIPPARD 1985 *Response and Stability: An Introduction to the Physical Theory.* Cambridge University Press.
15. M. S. HEIMAN, P. J. SHERMAN and A. K. BAJAJ *Journal of Sound and Vibration* On the dynamics and stability of an inclined impact pair.
16. J. GUCKENHEIMER and P. J. HOLMES 1983 *Nonlinear Oscillations, Dynamical Systems, and Bifurcations of Vector Fields* New York: Springer-Verlag.
17. A. E. KOBRINSKII 1969 *Dynamics of Mechanisms with Elastic Connections and Impact Systems.* London: Iliffe Books.
18. P. J. HOLMES and F. C. MOON 1983 *Journal of Applied Mechanics* **50**, 1021-1032. Strange attractors and chaos in nonlinear mechanics.

APPENDIX

In this appendix we demonstrate the utility of the results of sections 3. and 4 by investigating three specific steady state motions. These include $1:L$, $2:L$ and $3:1$ steady state impact sequences. The $1:L$ motion is most easily analyzed, and in fact, one can obtain explicit closed form expressions to characterize it. The $2:L$ motion is not amenable to such an explicit analysis, and illustrates, in principle, the type of approach that would be taken for a more general $K:L$ motions. The $3:1$ motion investigation is presented primarily to illustrate the extremely rich dynamics which are involved in such an apparently simple physical system.

A.1. $1:L$ MOTIONS

This section is concerned with $1:L$ motions in which the secondary mass m impacts only on the left end of the slot. This type of motion is similar to that described by Holmes [9] for a ball bouncing on a vertically vibrating horizontal table. Steady state motions require $\alpha_0 = \alpha_1 = 0$, $\alpha_2 = 2\pi L$, and $\dot{z}_2 = \dot{z}_0$. Since there is no unknown α term, the analysis is simplified. Solving the velocity equations derived from equations (7b) and (8b) yields

$$\dot{z}_0 = A\omega \cos(\theta)\cos(\tau) - \frac{2g\sin(\theta)}{1-e}\left[\frac{\pi L}{\omega}\right] \tag{A1a}$$

and

$$\dot{z}_1 = A\omega \cos(\theta)\cos(\tau) + \frac{2eg\sin(\theta)}{1+e}\left[\frac{\pi L}{\omega}\right]. \tag{A1b}$$

For this type of motion, equation (9) relates consecutive impacts on the same side of the slot, so that $\Delta y_1(d) = 0$. In this case, equations (9) and (A1b) simplify to the single constraint

$$\cos(\tau) = [(1-e)/(1+e))](\pi L/\gamma)\tan(\theta) \tag{A2}$$

where $\gamma = A\omega^2/g$ represents the normalized acceleration of the primary mass, M. Equation (A2) reveals that no more than two steady state $1:L$ motions may exist for any given set of system parameters. That the initial phase τ must lie in the interval $(-\pi/2, \pi/2)$ indicates that the secondary mass must impact the left end of the slot while the primary mass M is moving to the right. Since $\cos(\tau)$ is bounded by ± 1, equation (A2) gives the inequality constraint

$$\gamma \geqslant \gamma_{\min} = [(1-e)/(1+e)]\pi L \tan(\theta), \tag{A3}$$

which defines a solution existence boundary in the γ-θ plane for fixed e and L. Similar inequalities may also be developed for other pairs of combinations of the parameters γ, θ, e and L. We remark that under zero initial conditions the mass m will never leave the left end of the slot for $\gamma < \tan\theta$ for any $K:L$ motion. This fact does not contradict constraint (A3) in which non-zero initial conditions are assumed.

One can now proceed to investigate the stability of the $1:L$ motion defined by constraint (A2).

By using equations (14)-(17), it can be shown that

$$DP = \begin{bmatrix} 1 - \dfrac{(1+e)^2 A\omega^2 \sin(\tau)}{g\tan(\theta)} & \dfrac{-e\omega(1+e)}{g\sin(\theta)} \\ e(1+e)A\omega\cos(\theta)\sin(\tau) & e^2 \end{bmatrix}. \tag{A4}$$

Straightforward calculations of expression (A4) show that $\mathrm{Det}[DP] = e^2$, verifying equation (19). It also follows that the sum of eigenvalues of DP is

$$\mathrm{Tr}[DP] = 1 + e^2 - (1+e)^2 \sin(\tau)\gamma/\tan(\theta). \tag{A5}$$

It can be shown that $|\mathrm{Tr}[DP]|$ achieves its maximum value $1+e^2$ on the $\lambda_c = \pm 1$ stability boundaries, subject to $\mathrm{Det}[DP] = e^2$ and $|\lambda_1|, |\lambda_2| \leqslant 1$. Therefore, for the critical eigenvalue $\lambda_c = +1$, equation (A5) shows that $\rho = 0$. Substituting this value of τ into constraint (A2) results in $\gamma = \gamma_{\min}$, so that the existence boundary (A3) corresponds to the $\lambda_c = +1$ stability boundary in the γ-θ plane. The condition $\tau = 0$ at $\gamma = \gamma_{\min}$ indicates that in order to support stable $1:L$ motion for the minimum possible acceleration of M, the secondary mass m must impact the left end of the slot when M is midway in its travel to the right,

which is where its velocity is maximum. In a similar manner, $\lambda_c = -1$ yields the upper bound.

$$\gamma \leqslant \gamma_{\max} = \left\{4\left[\frac{1+e^2}{(1+e)^2}\right]^2 + \pi^2 L^2\left[\frac{1-e}{1+e}\right]^2\right\}^{1/2} \tan(\theta). \tag{A6}$$

From expressions (A3) and (A6) one can see that the range of accelerations of M, $\gamma_{\max} - \gamma_{\min}$ able to support stable $1:L$ motion is proportional to θ. As expected, no such motions are possible for $\theta = 0$.

The stability boundaries above can also be used to investigate how the range of values of the initial phase τ depends on the system parameters. As already noted, on the $\lambda_c = +1$ boundary $\tau = 0$. solving equation (A2) for γ and substituting this expression into equation (A5) for $\lambda_c = -1$ gives

$$\tan(\tau) = (2/\pi L)[(1+e^2)/(1-e^2)]. \tag{A7}$$

As $L \to \infty$, $\tau \to 0$, so that $\gamma_{\min} \to \gamma_{\max} \to \infty$. Thus, not only must the acceleration of M increase as the number L of cycles between impacts is increased, as one might expect, but the impacts must occur in the vicinity of the mid-point of the travel of M from left to right. This result also shows that the area of stable $1:L$ motions in the γ-θ plane decreases with increasing L.

The constraint equations and the stability equations are independent of the slot length d. However, d plays a role in determining the viability of the solution [cf., (11)].

A.2. $2:L$ MOTIONS

For this type of motion the secondary mass, m is assumed to impact at alternate ends of the slot. Such motions have been studied by several authors [1, 2, 4, 5, 8, 11, 14, 15] for various impacting systems. In this section the constraint and the stability equations will be derived for arbitrary L, but only 2:1 motions will be discussed in detail.

Since $K = 2$ there are 5 states, ranging from 0 to 4, required to specify the motion of m, $z(t)$, over L cycles of M. Steady state motion requires $\alpha_0 = \alpha_1 = 0$, $\alpha_4 = 2\pi L$, and $\dot{z}_4 = \dot{z}_0$. For notational convenience let $\alpha_2 = \alpha_3 \triangleq \alpha$. Then α represents the normalized time of flight between left and right impacts, or the proportion of the time taken in flight up the incline.

Solving the velocity equations derived from equations (7b) and (8b) for the $\dot{z}_i$'s gives

$$\dot{z}_1 = \frac{A\omega\cos(\theta)[\cos(\tau) - e\cos(\alpha+\tau)]}{1-e} + \frac{e(2\pi L - (1+e)\alpha)g\sin(\theta)}{\omega(1-e^2)} \tag{A8a}$$

and

$$\dot{z}_3 = -\frac{A\omega\cos(\theta)[e\cos(\tau) - \cos(\alpha+\tau)]}{1-e} - \frac{e[2e\pi L - (1+e)\alpha]g\sin(\theta)}{\omega(1-e^2)}. \tag{A8b}$$

It is not necessary to find expressions for $\dot{z}_0$ and $\dot{z}_2$ since the constraint and the stability equations do not involve them explicitly.

The alternating impact assumption implies that in equation (9) $\Delta y_1(d) = -d$ and $\Delta y_3(d) = d$. These, along with equation (A8) yield the following constraint equations: for $i = 1$,

$$-\frac{2}{\rho\cos(\theta)} + \frac{\alpha(4e\pi L - (1+e)^2\alpha)}{2\gamma(1-e^2)}\tan(\theta)$$

$$+\frac{\alpha}{1-e}[\cos(\tau) - e\cos(\alpha+\tau)] + \sin(\tau) - \sin(\alpha+\tau) = 0; \tag{A9a}$$

for $i=3$,

$$\frac{2}{\rho\cos(\theta)}-\frac{(2\pi L-\alpha)\{2(1+d^2)\pi L-(1+e)^2\alpha\}}{2\gamma(1-e^2)}\tan(\theta)$$

$$-\frac{(2\pi L-\alpha}{1-e}[e\cos(\tau)-\cos(\alpha+\tau)]-\sin(\tau)+\sin(\alpha+\tau)=0. \tag{A9b}$$

Here $\rho=2A/d$ is the ratio of the total displacement of M to the length of the slot, and $\gamma=A\omega^2/g$ is the ratio of the acceleration of M to gravity, as already defined for $1:L$ motions. The steady state $2:L$ motions are characterized by solutions $(\bar{\alpha},\bar{\tau})$ of the constraint equations (A9).

It is possible that more than one set of solutions satisfying equations (A9) exists for a given set of parameters. The solutions of physical interest are those which are at least locally stable. Equations (14), (16), and (17) permit computation of the explicit expressions

$$DP^{(0)}=\begin{bmatrix}1 & 0\\ -(1+e)A\omega\cos(\theta)\sin(\tau) & -e\end{bmatrix}, \tag{A10a}$$

$$DP^{(1)}=\begin{bmatrix}\dfrac{g\phi_1\tan(\theta)+e(1+e)A\omega^2C}{g\phi_1\tan(\theta)+(1+e)A\omega^2C} & \dfrac{-\alpha\omega(1-e^2)}{(g\phi_1\tan(\theta)+(1+e)A\omega^2C)\cos(\theta)}\\ \dfrac{A\omega g(1-e^2)\sin(\theta)C}{g\phi_1\tan(\theta)+(1+e)A\omega^2C} & \dfrac{eg\phi_2\tan(\theta)+(1+e)A\omega^2C}{g\phi_1\tan(\theta)+(1+e)A\omega^2C}\end{bmatrix}, \tag{A10b}$$

$$DP^{(2)}=\begin{bmatrix}1 & 0\\ -(1+e)A\omega\cos(\theta)\sin(\alpha+\tau) & -e\end{bmatrix}, \tag{A10c}$$

and

$$DP^{(3)}=\begin{bmatrix}\dfrac{g\phi_2\tan(\theta)+e(1+e)A\omega^2C}{g\phi_2\tan(\theta)+(1+e)A\omega^2C} & \dfrac{-(2\pi L-\alpha)\omega(1-e^2)}{\{g\phi_2\tan(\theta)+(1+e)A\omega^2C\}\cos(\theta)}\\ \dfrac{A\omega g(1-e^2)\sin(\theta)C}{g\phi_2\tan(\theta)+(1+e)A\omega^2C} & \dfrac{eg\phi_1\tan(\theta)+(1+e)A\omega^2C}{g\phi_2\tan(\theta)+(1+e)A\omega^2C}\end{bmatrix}, \tag{A10d}$$

where

$$\phi_1=2e\pi L-(1+e)\alpha,\qquad \phi_2=2\pi L-(1+e)\alpha\qquad\text{and}\qquad C=\cos(\tau)-\cos(\alpha+\tau).$$

By using these relations, it is straightforward to show that $\mathrm{Det}[DP]=e^4$, and that

$$\begin{aligned}\mathrm{Tr}[DP]=&[\phi_1\phi_2(1+e^4)\tan(\theta)^2+2e^2(1+e)^2\gamma^2C^2+4e^2(1+e)^2(\pi-\alpha)\gamma C\tan(\theta)\\ &+2e(1-e)(1+e)^3\pi\gamma^2C\{\sin(\tau)-\sin(\alpha+\tau)\}\\ &+(1-e)(1+e)^2\{2e^2\pi+(1-e^2)\alpha\}\phi_2\gamma\sin(\tau)\tan(\theta)\\ &-(1-e)(1+e)^2\{2\pi-(1-e^2)\alpha\}\phi_1\gamma\sin(\alpha+\tau)\tan(\theta)\\ &-(1-e)^2(1+e)^4\alpha(2\pi-\alpha)\sin(\tau)\sin(\alpha+\tau)]\\ &/[\{\phi_1\tan(\theta)+(1+e)\gamma C\}\{\phi_2\tan(\theta)+(1+e)\gamma C\}].\end{aligned} \tag{A11}$$

Even though equations (A10) and (A11) are too unwieldy to permit the type of stability analysis afforded the $1:L$ motion, for specified numerical values of the system parameters,

they provide a convenient means of ascertaining the stability of a $2:L$ motion characterized by $(\bar{\alpha}, \bar{\tau})$.

Since numerical evaluation of $2:L$ motions presented in section 6 was limited to 2:1 motions, we briefly consider the above results for the case $L=1$. Equations (A9) are non-linear with respect to the unknowns α and τ, so that numerical solutions of α and τ for 2:1 motions were obtained for a range of parameter sets $(\rho, \gamma, \theta, e)$ by using the IMSL routine ZSCNT. Typically, three different solution groups, based on the value of α, for $\alpha > \pi$, $\alpha < \pi$, and $\alpha = \pi$, were found. The $\alpha = \pi$ solutions are commonly referred to as equispaced solutions since the impacts are equispaced in time. If equations (A9) are added together, then for $\alpha = \pi$ the constraint

$$(1-e)\tan(\theta) = 0 \tag{A12}$$

is obtained. Since only energy dissipative ($e<1$) cases are considered, this implies that equispaced 2:1 motions exist only if $\theta = 0$. We remark that equation (A9) represents a direct extension of the equations of reference [11] for the inclined impact pair situation.

A.3. 3:1 MOTIONS

In this section only the equations associated with 3:1 motions are developed. As previously mentioned, one reason for considering this motion is to illustrate the extremely rich dynamics this system posseses. A second reason is that when 2:1 motions pass through a viability boundary simulation results show that they, in most cases, stabilize into 3:1 motions. We do not develop the $3:L$ case since, as the numerical results of section 6 have shown, the 3:1 motions are of sufficient complexity. There are two possible types of 3:1 steady state motions. The first includes two impacts on the left side before an impact on the right. We call this a LLR sequence. The second consists of one impact on the left followed by two impacts on the right. We call this a LRR sequence. The velocity equations and the stability equations for these LLR and LRR motions are identical, while the constraint equations differ with respect to the parameter $\Delta y_i(d)$ only.

For 3:1 motions, in one period the secondary mass has seven distinct states ranging from 0 to 6, where, in particular, $\alpha_0 = \alpha_1 = 0$, $\alpha_6 = 2\pi$, and $\dot{z}_6 = \dot{z}_0$. For notational convenience set $\alpha_2 = \alpha_3 = \alpha_I$ and $\alpha_4 = \alpha_5 = \alpha_{II}$. Again, equations (7b) and (8b) can be used to generate the required velocity equations:

$$\dot{z}_1 = \frac{e\{2\pi - (1+e)(\alpha_{II} - e\alpha_I)\} g \sin(\theta)}{\omega(1+e^3)} + \frac{A\omega \cos(\theta)\{\cos(\tau) - e\cos(\alpha_{II}+\tau) + e^2\cos(\alpha_I+\tau)\}}{1-e+e^2}, \tag{A13a}$$

$$\dot{z}_3 = -\frac{e\{2\pi - (1+e)[(1-e)\alpha_I + e\alpha_{II}]\} g \sin(\theta)}{\omega(1+e^3)} + \frac{A\omega \cos(\theta)\{\cos(\alpha_I+\tau) - e\cos(\tau) + e^2\cos(\alpha_{II}+\tau)\}}{1-e+e^2}, \tag{A13b}$$

$$\dot{z}_5 = \frac{e\{2e^2\pi - (1+e)[\alpha_I - (1-e)\alpha_{II}]\}}{\omega(1+e^3)} + \frac{A\omega \cos(\theta)\{\cos(\alpha_{II}+\tau) - e\cos(\alpha_I+\tau) + e^2\cos(\tau)\}}{1-e+e^2}. \tag{A13c}$$

The constraint derived from equations (9) and (A13) are

$$\left[\frac{\alpha_I}{1-e+e^2}\right][\cos(\tau)-e\cos(\alpha_{II}+\tau)+e^2\cos(\alpha_I+\tau)]$$
$$+\frac{\alpha_I\{4e\pi-(1+e)[\phi_-\alpha_I+e\alpha_{II}]\}}{2\gamma(1+e^3)}\tan(\theta)$$
$$+\sin(\tau)-\sin(\alpha_I+\tau)+\nu_1=0, \tag{A14a}$$

$$\left[\frac{\alpha_{II}-\alpha_I}{1-e+e^2}\right][\cos(\alpha_I+\tau)-e\cos(\tau)+e^2\cos(\alpha_{II}+\tau)]$$
$$-\frac{(\alpha_{II}-\alpha_I)\{4e^2\pi-(1+e)(\phi_+\alpha_I-\gamma_-\alpha_{II})\}}{2\gamma(1+e^3)}\tan(\theta)$$
$$+\sin(\alpha_I+\tau)-\sin(\alpha_{II}+\tau)+\nu_3=0, \tag{A14b}$$

$$\left[\frac{2\pi-\alpha_{II}}{1-e+e^2}\right][\cos(\alpha_{II}+\tau)-e\cos(\alpha_I+\tau)+e^2\cos(\tau)]$$
$$-\frac{(2\pi-\alpha_{II})\{2(1-e_3)\pi+(1+e)(2e\alpha_I-\phi_+\alpha_{II})\}}{2\gamma(1-e^3)}\tan(\theta)$$
$$+\sin(\alpha_{II}+\tau)-\sin(\tau)+\nu_5=0, \tag{A14c}$$

where $\phi_+=1+e-e^2$, $\phi_-=1-e-e^2$, and the ν_i's depend upon the impact sequence. If the motion is a LLR sequence then $\nu_1=0$, $\nu_3=-2/\rho\cos(\theta)$, and $\nu_5=2/\rho\cos(\theta)$. If the motion is a LRR sequence then $\nu_1=-2/\rho\cos(\theta)$, $\nu_3=0$, and $\nu_5=2/\rho\cos(\theta)$.

Equations (A14) are the desired non-linear equations whose solutions α_I, α_{II}, and τ determine, for a given parameter set, the possible 3:1 motions of the assumed type. These equations were solved by using the IMSL routine ZSCNT.

The stability of a given steady state 3:1 motion is determine by the Jacobian matrix DP specified in equation (15b), which depends on the matrices $DP^{(i)}$. Explicit expressions for these matrices may be computed from equations (16), (17) and (A14), but are not given here due to their length and complexity. Viability limits for the 3:1 motions may be evaluated by using equation (11), or as in section 7, where an alternative approach for finding the viability boundaries was developed.